Modeling the spatially distributed nature of subglacial sediment transport and erosion

Ian Delaney[1], Leif Anderson[1,2], and Frédéric Herman[1]

[1]Institut des dynamiques de la surface terrestre (IDYST), Université de Lausanne, Bâtiment Géopolis, CH-1015 Lausanne
[2]Department of Geology and Geophysics, University of Utah, Frederick Albert Sutton Building, 115 S 1460 E, Salt Lake City, UT 84112-0102, USA

Correspondence: Ian Delaney (IanArburua.Delaney@unil.ch)

Abstract. In addition to ice and water, glaciers expel sediment. As a result, changing glacier dynamics and melt result in changes to glacier erosion and sediment discharge, which can impact the landscape surrounding retreating glaciers, as well as communities and ecosystems downstream. To date, available models that transport subglacial sediment on sub-hourly to decadal scales are in one dimension, usually along a glacier's flow line. Such models have proven useful in describing the formation of landforms, the impact of sediment transport on glacier dynamics, and the interactions among climate, glacier dynamics, and erosion. However, these models omit the two-dimensional spatial distribution of sediment and its impact on sediment connectivity, i.e. the movement of sediment between its detachment in source areas and its deposition in sinks. In turn, there is a need for modeling frameworks that describe subglacial sediment discharge in two spatial dimensions (x and y) over time. Here, we present SUGSET_2D, a numerical model that evolves a two-dimensional subglacial till layer in response to bedrock erosion and changing sediment transport conditions below glaciers. Experiments performed using an idealized alpine glacier illustrate the heterogeneity in sediment transport and bedrock erosion below glaciers. The experiments show an increase in sediment discharge following increased glacier melt, as has been documented in field observations and other numerical experiments. We also apply the model to a real alpine glacier. Model outputs are compared with annual observations of sediment discharge measured from Griesgletscher in the Swiss Alps. SUGSET_2D reproduces general quantities of sediment discharge and the year-to-year sediment discharge pattern measured at the glacier terminus. The model's ability to match the data depends greatly on the sediment grain size parameter, which controls subglacial sediment transport capacity. Smaller grain sizes allow sediment transport to occur in regions of the bed with reduced water flow and channel size, effectively increasing sediment connectivity into the main channels. Model outputs from both cases show the importance of considering spatial heterogeneities in water discharge and sediment transport in both the x- and y- dimensions in evaluating sediment discharge from glaciers.

1 Introduction

Increasing glacier ablation perturbs the ways that glaciers erode bedrock and supply sediment downstream (e.g., Church and Ryder, 1972; Lane et al., 2017; Delaney and Adhikari, 2020). Changing sediment discharge from glaciers in alpine and polar landscapes impacts many downstream social and earth systems (Milner et al., 2017; Li et al., 2021). In turn, predictive models are needed to understand the response of these systems to glacier retreat. In alpine environments, increased sediment discharge leads to the more rapid filling of proglacial reservoirs (Thapa et al., 2005; Li et al., 2022) and abrasion of hydropower infrastructure (e.g. Felix et al., 2016). The flux of sediment from glaciers also dramatically alters alpine ecosystems (Milner et al., 2017). In the Arctic, increased sediment discharge can affect biogeochemical cycles given that sediments may carry phosphorus and iron (Bhatia et al., 2013; Hawkings et al., 2014). These elements are limiting nutrients in the oceanic ecosystem, so any change to sediment discharge from the ice sheet can alter Arctic ecosystems (Wadham et al., 2019). Modeling studies and observations suggest that increases in sediment output from alpine glaciers could occur when high melt extends up-glacier, mobilizing sediment in new areas (Lane et al., 2017; Delaney and Adhikari, 2020; Li et al., 2021).

Generally, two processes determine the sediment discharge below glaciers: one process adds sediment, the other removes sediment from subglacial till layers (Figure 1; Brinkerhoff et al., 2017; Delaney et al., 2019). Bedrock erosion adds material to the subglacial till layer. Bedrock erosion is accomplished by quarrying, when pressure differentials on opposing sides of obstacles cause fractures to expand and rock to detach (Iverson, 1990; Alley et al., 1997; Hallet et al., 1996; Iverson, 2012), and abrasion, when debris embedded in the ice grinds bedrock as the glacier slides above (Hallet, 1979; Alley et al., 1997). Representing these physical processes in models requires independent knowledge of a large number of parameters (c.f. Ugelvig et al., 2018), so many researchers use empirical relationships that relate glacier sliding to glacier erosion (Humphrey and Raymond, 1994; Koppes et al., 2015; Herman et al., 2015; Cook et al., 2020). The sliding relationship with glacier erosion proves especially useful when applied over large temporal and spatial scales, for example, to explore the coupling of glacier erosion, climate, and tectonic uplift (e.g., Egholm et al., 2009; Prasicek et al., 2018; Herman et al., 2018; Prasicek et al., 2020; Seguinot and Delaney, 2021).

Conversely, fluvial sediment transport mobilizes material from subglacial till layers (e.g., Walder and Fowler, 1994; Ng, 2000; Creyts et al., 2013), or may deposit it there under certain hydraulic conditions (e.g., Beaud et al., 2018b). When subglacial water velocity increases above a critical threshold, sediment of a given grain size is transported downglacier, and if the water velocity slows below the threshold, sediment may be deposited (Shields, 1936). The sediment mobilization ceases when no sediment is present, and the system is supply- limited (e.g., Mao et al., 2014). It follows that fluvial sediment transport depends on both the subglacial hydraulic characteristics (e.g., Walder and Fowler, 1994), and the the availability of sediment at the glacier bed (e.g., Willis et al., 1996; Swift et al., 2005).

Bedrock erosion and fluvial sediment transport vary depending on the characteristics of each glacier. Bedrock erosion processes tend to dominate sediment discharge below glaciers with minimal sediment storage, large concentrations of subglacial debris entrained at the glacier bed and steep gradients (Hallet, 1979; Humphrey and Raymond, 1994; Herman et al., 2015; Ugelvig et al., 2018; Herman et al., 2021). Landscape evolution models that represent glacier landscapes illustrate the dominant role of erosional processes, as opposed to sediment transport processes, over geologic timescales (Harbor et al., 1988; Herman et al., 2011; Egholm et al., 2012). Over shorter timescales of months to decades fluvial sediment transport often drives sediment discharge from glaciers (e.g., Delaney et al., 2018b; Perolo et al., 2018; Delaney et al., 2019).

The development of numerical models of subglacial sediment transport has thus far focused on processes acting a single downglacier (e.g., x-) dimension. Yet, the spatial heterogeneities in the distribution of sediment and sediment transport capacity (largely controlled by water velocity) often result in less sediment being carried by the water than could be transported theoretically (e.g., Lane et al., 2017; Delaney et al., 2018b). As a result, reducing the problem to one dimension omits key processes controlling sediment dynamics because subglacial water flows through spatially distributed networks of cavities and channels across the glacier bed (e.g., Werder et al., 2013). To date, the one-dimensional models have yielded insights into the creation of eskers (Beaud et al., 2018a; Hewitt and Creyts, 2019), the formation of subglacial canals through which water flows (Walder and Fowler, 1994; Ng, 2000; Kasmalkar et al., 2019), subglacial processes in overdeepenings (Creyts et al., 2013) and the behavior of tidewater glaciers (Brinkerhoff et al., 2017). Yet, describing subglacial sediment transport inherently lends itself to a discretization of bedrock erosion, sediment transport, water flow, and sediment availability in both the downglacier and transverse dimensions (e.g., x- and y-).

In this manuscript, we present SUGSET_2D, a two-dimensional subglacial sediment transport model. The model includes subglacial sediment transport and bedrock erosion processes. We implement a routing scheme that transports sediment in x- and y- based on the local hydraulic potential gradient. Synthetic cases demonstrate the model's ability to reproduce known processes and yield insight into the spatially-distributed processes responsible for subglacial sediment dynamics. We also apply the model to a real alpine glacier, Griesgletscher in Switzerland. The model was run with hydrology and topography data from the glacier, and measured sediment discharge data were used to validate the model. Through these experiments, we explore the importance of two-dimensional sediment connectivity in the subglacial environment.

2 Model Description

The model presented here implements a hydraulic model and sediment routing scheme that translates many of the underpinnings of the one-dimensional subglacial sediment transport model presented in Delaney et al. (2019) to two dimensions. In this section, we describe hydraulic and sediment transport models, explain the implemented water and sediment routing scheme, and outline its numerical implementation in two dimensions.

2.1 Hydraulic Model

SUGSET_2D requires a hydraulic model as a means to route sediment and water through the subglacial environment. The hydraulic model is also needed to evaluate the sediment transport capacity of this water, based upon the hydraulic gradient, channel size, and water flux (Table 1, Section 2.2; e.g., Walder and Fowler, 1994; Alley et al., 1997). The hydraulic model is based on the premise that subglacial water flows along the hydraulic potential gradient and the weight of ice pressurizes water at the bed (Shreve, 1972). This model includes characteristics of an Röthlisberger-channel without explicitly describing properties such as creep closure and pressure melt of channel walls.

The hydraulic gradient of a subglacial channel Ψ (at a certain location and time) can be determined with a known hydraulic diameter D_h and water discharge Q_w. The hydraulic gradient can then be determined using the Darcy-Weissbach equation for fluid flow through a pipe

$$\Psi = s\, f_r\, \rho_w\, \frac{Q_w^2}{D_h^5} \quad , \tag{1}$$

the density of water is ρ_w, the Darcy-Weisbach friction factor is f_r, and the channel's cross-sectional geometry, which impacts water pressure, is accounted for by s (Hooke et al., 1990). We represent s as

$$s = \frac{2\,(\beta - \sin\beta)^2}{(\frac{\beta}{2} + \sin\frac{\beta}{2})^4} \quad , \tag{2}$$

where β is the central angle of the circular segment representing the channel edge. Smaller values of β result in broad channels and $\beta = \pi$ results in a semicircular channel.

To approximate the hydraulic diameter D_h, we prescribe a melt rate $\dot{m}_w$ to establish Q_w and assign a representative water discharge Q_w^* to Q_w, by taking a characteristic water discharge over a certain time period prior (hours to days). We assume that the hydraulic diameter of the channel results from this characteristic water discharge we call the source percentile (s_p; c.f. Gimbert et al., 2016; de Fleurian et al., 2018; Delaney et al., 2019; Nanni et al., 2020). The response time, s_a and source percentile, s_p, remain consistent throughout the model run. The values for these variables are poorly constrained, yet their impact can be intuited. For instance, short-lived increases in water discharge due to an hour of precipitation will not greatly impact the hydraulic diameter of the subglacial channel, whereas prolonged melt would increase the hydraulic diameter.

Q_w^* and Q_w comprise the total instantaneous amount of melt water produced upglacier, as this hydraulic model does not consider water storage.

D_h, the hydraulic diameter is evaluated from

$$D_h = \left(s\, f_r\, \rho_w\, \frac{Q_w^{*\,2}}{\Psi^*}\right)^{\frac{1}{5}} \quad . \tag{3}$$

Ψ^* is a representative hydraulic gradient at overburden pressure, evaluated using the Shreve potential gradient

$$\Psi^* = \nabla(\rho_i\, g\,(z_s - z_b) + \rho_w\, g\, z_b) \quad , \tag{4}$$

where z_s and z_b are surface and bed elevations, respectively, ρ_i is the density of ice and g is the gravitational acceleration constant.

With knowledge of D_h, we insert the instantaneous value of Q_w into Equation 1 to evaluate the instantaneous hydraulic gradient Ψ. To prevent unreasonable water pressures when Q_w^* rapidly increases and D_h is small, the model limits the minimal hydraulic diameter to $0.3\,\mathrm{m}$ (Delaney et al., 2019).

2.2 Till layer model: bedrock erosion and sediment transport

The model simulates the evolution of a subglacial till layer, which we define as transportable sediment below the glacier due to glacier erosion and fluvial sediment transport. Fluvial sediment transport, in supply- and transport-limited regimes, mobilizes and deposits sediment, adding or removing material from the till layer (Brinkerhoff et al., 2017; Delaney et al., 2019). Conversely, erosive processes such as abrasion and quarrying add material to the layer, while we do not consider processes such as fluvial abrasion that appear to produce minimal sediment (Beaud et al., 2018b). To represent these processes, we implement the Exner Equation (Figure 2; Exner, 1920a,b; Paola and Voller, 2005), a mass conservation relationship, to solve for the till layer height given the erosive and fluvial conditions.

$$\underbrace{\frac{\partial H}{\partial t}}_{\text{till evolution}} = - \underbrace{\nabla \cdot Q_s}_{\text{sediment transport}} + \underbrace{\dot{m}_t}_{\text{bedrock erosion}} , \tag{5}$$

H is till thickness and t is time (Table 1). The first term represents fluvial sediment transport processes, where $\nabla \cdot Q_s$ represents sediment mobilization in either supply- or transport- limited regimes. The second term captures bedrock erosion processes, where $\dot{m}_t$ is a bedrock erosion rate.

We evaluate the mobilization of sediment in both supply- and transport- limited conditions. Divergence of the sediment flux is evaluated by approximating $\nabla \cdot Q_s$ with $\frac{\nabla \cdot \widetilde{Q_s}}{w}$ and using the mobilization scheme from Delaney et al. (2019)

$$\nabla \cdot \widetilde{Q_s} = \begin{cases} \dfrac{Q_{sc} - Q_s}{l} & \text{if } \frac{Q_{sc}-Q_s}{l} \leq \dot{m}_t w \quad \text{(transport-limited)} \quad (6a) \\ 0 & \text{if } H = H_{lim} \quad \& \quad \frac{Q_{sc}-Q_s}{l} \leq 0 \quad (6b) \\ \dfrac{Q_{sc} - Q_s}{l}\,\sigma(H) + \dot{m}_t w\,(1 - \sigma(H)) & \text{otherwise} \quad \text{(supply-limited)} \quad (6c) \end{cases}$$

w is the width of a patch of glacier bed perpendicular to the direction of water flow overwhich sediment can be accessed by a channel. Q_{sc} is sediment transport capacity, or the amount of sediment that could be transported under the given hydraulic conditions. l is a characteristic length-scale for sediment mobilization, over which sediment mobilization adjusts to sediment transport conditions. σ is a sigmoidal function of H

$$\sigma(H) = \left(1 + \exp\left(\frac{2 - \Delta\sigma H}{5}\right)\right)^{-1}, \tag{7}$$

which enables smooth transition from transport- to supply- limited transport in Equation 6c. If H is greater than $3\,\Delta\sigma$, then sediment mobilization is unaffected and the system is in a transport-limited regime. When $H = \Delta\sigma$, then $\sigma(H)$ is close to 0, sediment transport is in a supply-limited regime, and nearly no sediment mobilization takes place.

Condition 6a represents the case where bedrock erosion exceeds sediment mobilization, thus sediment transport exists in a transport- limited regime. Condition 6b impedes mobilization or deposition, transporting sediment to the next cell when a till thickness is equal to H_{lim}, the value of which is chosen to be on the order of maximal change in till height over the model run ($\sim 10\,\mathrm{cm}$). This term prevents unbounded sediment accumulation, as the model does not include physical processes to limit sediment deposition, such as reduced channel size in response to infill of sediment (Perolo et al., 2018). Condition 6c allows sediment mobilization to transition between transport- and supply-limited regimes, limiting sediment mobilization to sediment production term $\dot{m}_t$ (see below), when H is small and thus minimal sediment is available for transport. With these three conditions, we can evaluate sediment transport in transport- and supply-limited regimes and pass sediment through the system when till height is large.

We calculate sediment transport capacity Q_{sc} using the total sediment transport relationship by Engelund and Hansen (1967),

$$Q_{sc} = \frac{0.4}{f_r} \; \frac{1}{D_m(\frac{\rho_s}{\rho_w} - 1)^2 g^2} \; \left(\frac{\tau}{\rho_w}\right)^{\frac{5}{2}} w_c \;\; , \tag{8}$$

where ρ_s (ρ_w) is the bulk density of the sediment (water), D_m is the mean sediment grain size and τ represents the shear stress between the water and the channel bed.

The width of the channel floor w_c, needed to evaluate the surface over-which sediment transport may occur, is given by

$$w_c = 2\sin\frac{\beta}{2}\sqrt{\frac{2\,S}{\beta - \sin\beta}} \;\; , \tag{9}$$

where again β is the Hooke angle controlling channel morphology (Section 2.1), S is the cross-sectional area of the channel given by

$$S = \frac{D_h^2}{2} \, \frac{\left(\frac{\beta}{2} + \sin\frac{\beta}{2}\right)^2}{\beta - \sin\beta} \;\; . \tag{10}$$

Here, hydraulic diameter D_h is evaluated from Equation 3.

We also determine the shear stress in Equation 8 through the Darcy-Weisbach

$$\tau = \frac{1}{8}\, f_r \,\rho_w \, v^2 \;\; , \tag{11}$$

where $v = \frac{Q_w}{S}$ is the water velocity. Water discharge Q_w is calculated by the water flowing above and S is evaluated in Equation 10. Other sediment transport relationships using shear stress could be exchanged by the model operator (e.g., Meyer-Peter and Müller, 1948). We chose Engelund and Hansen (1967)'s formulation due to the representation of both suspended and bedload transport.

We assume that till armors the bed from erosion (e.g., Alley et al., 2003; Brinkerhoff et al., 2017; Delaney et al., 2019). In response, the source term $\dot{m}_t$ is described as,

$$\dot{m}_t = \dot{e}\left(1 - \frac{H}{H_{max}}\right) \;\; , \tag{12}$$

where H_{max} is a till height beyond which no further erosion, $\dot{e}$, may occur.

We chose to use an empirical relationship with sliding velocity u_b to describe bedrock erosion,

$$\dot{e} = k_g \, {u_b}^{l_{er}} \;\; , \tag{13}$$

where k_g is an erodability constant and l_{er} is an exponent, which varies from between 0.66 and 3 (Herman et al., 2021). u_b is assumed to be related to basal shear stress (τ_b; Weertman, 1957) given the following relationship

$$u_b = B\tau_b^m \;\; , \tag{14}$$

B is a constant and we assume the exponent m is equal to 1. We assume that τ_b is equal to driving stress (Cuffey and Paterson, 2010)

$$\tau_b = \rho_i \, g \, h \, (\sin\alpha) \quad , \tag{15}$$

where ρ_i is the density of ice, h is the glacier thickness, and α is the surface slope of the glacier.

Note that alternative parameterizations of erosion or basal sliding can easily be exchanged for $\dot{m}_t$.

2.3 Spatial and temporal discretization, and parameters

Here, we describe the numerical implementation of the equations presented above, and in particular the routing scheme that enables a two-dimensional representation of subglacial fluvial and till dynamics.

2.3.1 Water and sediment routing and implementation

We assume that sediment and water moves across the glacier bed following the steepest gradient in hydraulic potential. On glaciers, we define the hydraulic potential at a cell i in the grid, ϕ_i, based upon the elevation of the glacier bed plus the ice thickness, following Shreve (1972).

$$\phi_i = f_f \, \rho_i \, g \, (z_{s,i} - z_{b,i}) + \rho_w \, g \, z_{b,i} \quad , \tag{16}$$

where f_f is the flotation fraction across the glacier, z_s is the glacier surface, and z_b is the glacier bed.

With this information, we use a multi-cell routing scheme (Quinn et al., 1991) to establish flow routing based upon the steepest hydraulic potential in Equation 16 and with a single value of f_f across the glacier bed. We implement this scheme in a similar way as Bovy et al. (2016), but on a regular grid in x and y directions, where fluxes can pass to the four surrounding cells sharing an edge. This routing scheme returns a stack (s_t; Table 3), which contains information about the order of cells to perform the calculations, along with the number of cells flowing in to a cell (donors; n_d), number of cells that a cell contributes (receivers; n_r), and the weight of hydraulic potential and water or sediment discharge directed from one cell to another (w_d or w_r).

For the first time step, the hydraulic potential ϕ is evaluated under the condition that $f_f = 1$. After the first time step, we assume that the flotation fraction, will vary in response to changing hydraulic conditions such as diurnal or seasonal water input (e.g., Iken and Bindschadler, 1986). In turn, to establish an average flotation fraction f_f across the glacier bed for Equation 16, we use

$$f_f = \mathrm{mean}\left(\frac{\phi_{o,i}}{\rho_i \, g \, (z_{s,i} - z_{b,i}) + \rho_w \, g \, z_{b,i}} \right) \quad , \tag{17}$$

where the denominator represents the hydraulic potential at overburden pressure ($f_f = 1$ in Equation 16).

ϕ_0 represents the hydraulic potential evaluated from summing the hydraulic gradient Ψ in Equation 1 up glacier from its outlet. ϕ_0 at each cell i is evaluated as

$$\phi_{o,i} = \Psi_i \cdot \lambda + \sum_{j=1}^{n_r} (\phi_{0,j} \cdot w_{r,j}) \quad . \tag{18}$$

Here, Ψ_i comes from evaluating Equation 1 from the receiver cell j of i, λ is edge length of a cell on a regular grid, n_r is the number of receivers that the cell i has, and w_r is the proportion of hydraulic potential fed by the upstream cell j. The operation is executed on a cell by cell basis, beginning at the base of the glacier and moving up the flow paths evaluated in the routing scheme.

Using the routing scheme above, but performing the operation from the top of the glacier, we evaluate the water discharge in a cell $Q_{w,i}$ from melt upstream as

$$Q_{w,i} = \dot{m}_{w,i} \cdot \delta + \sum_{j=1}^{n_d} Q_{w,j} \cdot w_{d,j} \quad , \tag{19}$$

where $\dot{m}_w$ is a prescribed meltwater source term in cell i, n_d is the number of cells directing water at cell i, and $w_{d,j}$ is the percentage of water flow from cell j directed at cell i.

Sediment mobilization into a cell $\overline{Q_{s,i}}$ is like-wise computed by implementing Equation 6 from the top of the glacier through the stack as

$$\overline{Q_{s,i}} = \begin{cases} \sum_{j=1}^{n_d} \left(\frac{Q_{sc,j} - Q_{s,j}}{l} \cdot w_{d,j} \right) & \text{if } \sum_{j=1}^{n_d} \left(\frac{Q_{sc,j}-Q_{s,j}}{l} \right) \cdot w_{d,j} \leq \dot{m}_{t,i} \cdot \lambda \quad \text{(20a)} \\ 0 & \text{if } H_j = H_{lim} \quad \& \quad \frac{Q_{sc,j}-Q_{s,j}}{l} \leq 0 \quad \text{(20b)} \\ \dot{m}_{t,i} \lambda \, (1 - \sigma(H)) + \sum_{j=1}^{n_d} \left(\frac{Q_{sc,j} - Q_{s,j}}{l} \right) \cdot \sigma(H) \, w_{d,j} & \text{otherwise} \quad \text{(20c)} \end{cases}$$

where $Q_{sc,j}$ is the sediment transport capacity from cell j flowing to i, $Q_{s,j}$ is sediment discharge entering from cell j to cell i, again l is a response length scale and λ is cell length.

Sediment discharge $Q_{s,i}$ out of a cell i is evaluated as

$$Q_{s,i} = \overline{Q_{s,i}} \cdot \lambda + \sum_{j=1}^{n_d} Q_{s,j} \quad . \tag{21}$$

We evaluate the change in till height at a cell by implementing Equation 5 as

$$\frac{dH_i}{dt} = \frac{-Q_{s,i} + \sum_{j=1}^{n_d} Q_{s,j}}{\delta} + \dot{m}_{t,i} \quad , \tag{22}$$

where again δ is cell area.

2.3.2 Numerics and parameters

Spatial discretization on the regular grid must be substantially smaller than characteristic length-scale, l, in Equations 6 and 20. We then solve Equation 22 to establish till height H for given initial and boundary conditions in response to till production $\dot{m}_t$ and divergence of the sediment discharge Q_s using an explicit time integration scheme.

To discretize the problem in time, the model implements the VCABM solver (Hairer et al., 1992; Radhakrishnan and Hindmarsh, 1993) from the package *DifferentialEquations.jl* (Rackauckas and Nie, 2017) to evolve till layer height H. This solver implements an adaptive time step and uses a linear multistep method (Adams-Moulton) that is well-suited to non-stiff problems, which is optimal because of the rapid fluctuations in sediment transport that can occur. We impose a maximum time step of $6\,\mathrm{h}$ to ensure that the model captures the response to diurnal variations in melt input. In practice, the solver commonly uses a time step of roughly 20 minutes, which varies depending on sediment transport conditions and solver tolerance. Longer time steps occur over periods when glacier melt, and thus sediment transport, cease (i.e. winter months). Table 3 presents the numerical parameters used.

We execute the routing scheme based upon hydraulic conditions to the nearest 6 minutes to improve stability and fill closed basins in hydraulic potential to maintain continuous sediment transport through the domain. Smaller solving tolerances increase the computational time due to 1) increased accuracy of the solution and 2) the reassessment of flow fractions between the adjacent cells, which results in different routing configurations as the model converges.

We impose boundary conditions on the edge cells so no sediment or water enters the domain. At outlet cells, water discharge leaves the domain, as does a flux of sediment, based on sediment transport conditions. In other applications, boundary conditions could also be set to represent processes, such as hillslope erosion or glacial lakes, that route sediment or water to the subglacial environment (e.g., Andersen et al., 2015). At the outlet cells, we assume that the hydraulic potential has no ice overburden pressure.

Evolving Equation 5 requires an initial till height, H_0, chosen by the model user. This initial till height represents material from bedrock erosion created prior to the model initialization. We apply a "spin up" procedure to create a reasonable relationship between the amount of fluvial sediment transport and bedrock erosion.

New versions of the code are tested against reference cases to ensure consistency. Additionally in each test, we ensure mass conservation by checking that the amount of sediment leaving the system through fluvial transport is consistent with the till height change and erosion occurring under the simulated glacier.

3 Model Application

We use two cases to highlight model viability under increasingly complex situations. First, we apply the model to a synthetic alpine glacier topography with a synthetic hydrologic forcing, based on the Subglacial Hydrology Model Inter-comparison Project (SHMIP; de Fleurian et al., 2018), to illustrate the model's performance in a simplistic scenario. We then apply the model to the topography, and sediment and water discharge at Griesgletscher in the Swiss Alps. We demonstrate the proficiency of the model by comparing sediment transport model output and data (Delaney et al., 2018a). We also identify some drivers of subglacial sediment discharge in the model from these simulations.

3.1 Synthetic alpine cases

3.1.1 Experiment design

We run simulations using an alpine glacier geometry, along with the seasonally and diurnally varying hydrological forcing from the SHMIP project experiments (de Fleurian et al., 2018)). The domain is $6000\,\mathrm{m}$ on one axis and $1080\,\mathrm{m}$ on the other. The resulting geometry approximates the Bench Glacier in Alaska. The U-shaped bed and variable ice thickness mean that variable hydrologic gradients will occur laterally across the glacier and water can be routed across multiple cells.

To represent hydrology that varies over seasonally and diurnally, we implement a simple spatially distributed melt model, as in SHMIP (de Fleurian et al., 2018)

$$\dot{m}_w(z_s) = \begin{cases} M_f T(z_s) + \dot{m}_b & \text{if } T(z_s) > 0 \\ \dot{m}_b & \text{if } T(z_s) \leq 0 \end{cases}, \tag{23}$$

where $M_f = 0.01\,\mathrm{m\,K^{-1}\,d^{-1}}$ is a melt factor, and $\dot{m}_b$ is the basal melt rate. $T(z_s)$ is air temperature T at elevation z_s, defined as

$$T(z_s) = \left(-A_a \cos\left(\frac{2\pi t}{s_{year}}\right) + A_d \cos\left(\frac{2\pi t}{s_{day}}\right) + \Delta T - 5\right) \cdot \left(1 + z_s \frac{dT}{dz}\right), \tag{24}$$

where A_a and A_d are the annual and diurnal amplitudes in temperature, respectively; ΔT is a temperature offset, which is adjusted to control the meltwater input; s_{day} are the number of seconds in one day; s_{year} is the number of seconds in a year; $\frac{dT}{dz} = -0.0075\,\mathrm{K\,m^{-1}}$ is the air temperature lapse rate. In this case, we route water directly to the subglacial system at the location where the melt occurs, for instance, omitting moulins or crevasses that concentrate meltwater delivery to the bed.

We run the model for 10 years with a steady climate, then we apply a linear temperature increase of $0.5°\ \mathrm{a}^{-1}$ for 10 years followed by 10 years of steady temperature at the maximal ΔT. We implement the dramatic warming to capture the model's response to variable climatic conditions. The model is initiated with $5\,\mathrm{cm}$ of till across the bed. To spin up the model, we apply the initial year of hydrological forcing for $5\,\mathrm{a}$ for computational reasons. In other applications the spin up could be maintained, until the annual change in till height was well below commonly accepted glacier erosion rates (Hallet et al., 1996).

3.1.2 Model outputs and findings

Simulations show that over seasonal timescales, sediment discharge increases at the onset of melt and decreases shortly thereafter, prior to the maximum amount of water discharge that occurs in the peak of each melt season (Figure 4). Daily-averaged sediment discharge decreases until the very end of the melt season, when sediment discharge increases very slightly again (Figure 5 b, d, f). This occurs when water stops flowing during the night, allowing sediment to accumulate in the channels from bedrock erosion. Increased sediment discharge at the beginning of the melt season results from greater sediment availability following the growth of the till layer over the winter months, when the small amount of melt prevents substantial transport sediment. Increases in sediment discharge at the onset of melt produced by the model (Figure 4 b, and 5 b, d, f) have been observed for real glaciers (Willis et al., 1996; Swift et al., 2005; Riihimaki et al., 2005; Delaney et al., 2018b) and reproduced in the one-dimensional version of this model (Delaney et al., 2019).

Over the course of the simulation, the mean till height continues to decrease throughout the model run (Figure 4 a) . Exhaustion of sediment is evident in the middle of the glacier where much of the water flows resulting from the spin up procedure (Figure 6 e f). However, the decreasing till height through the model run results from mobilization on the margins of the glacier, where water flow in a warmer climate occurs more often. Increased water flow on the upper reaches of the glacier results in increased sediment transport (Figure 4 b) and a greater area of the bed were sediment transport occurs (Figure 6 e, f).

For the cases described above, bedrock erosion relies only on driving stress and till thickness. Sliding and bedrock erosion did not vary seasonally with increased subglacial water discharge (Figure 4 a). This causes sediment to accumulate during the winter months, which subsequently provides ample material for transport when melt increases in the spring. To test the effects of spatially variable erosion and the role of hydrology, we present two additional cases to supplement the alpine glacier case above, *ORIGINAL*. One additional case, *SEASON*, simulates bedrock erosion by only allowing sliding, and thus erosion, during the summer months (e.g., Iken and Bindschadler, 1986); the same erosion relationship is applied as the case in Section 3.1. In this case, however, erosion only occurs when the amount of water input substantially exceeds the background basal melt input rate, that is present in the winter. We choose this case to capture the seasonal variations in bedrock erosion (Ugelvig et al., 2018). In the other additional case, *CONST*, bedrock erosion remains constant over the entirety of the glacier at a rate of $2\,\mathrm{mm\,a^{-1}}$, independent of glacier sliding velocity.

The *ORIGINAL* case discharges over $11,620\,\mathrm{m^3}$ of sediment per year, while the *SEASON* case discharges only 60% of that value due to the absence of bedrock erosion during the winter months. The *CONST* case discharged $7320\,\mathrm{m^3}$ of sediment over the year. *CONST*'s quantity of sediment discharge results in a catchment-scaled height change roughly $1.1\,\mathrm{mm\,a^{-1}}$ due to decreased erosion efficiency with till height (Equation 12), instead of prescribed bedrock erosion rate of $2\,\mathrm{mm\,a^{-1}}$. Additionally, the spatial disparity of where sediment is produced at the glacier bed compared to the location of sediment transport further reduces the catchment scaled height change (Figure 6 e, f).

Over the three cases, sediment discharge increases at the onset of melt and substantially decreases by the end of the melt season due to sediment exhaustion. In *ORIGINAL* (Figure 5 a, b), more sediment discharge occurs compared to the alternate cases (*SEASON* and *CONST*). The increased sediment discharge in *ORIGINAL* is 1) due to the prolonged period over which bedrock erosion occurs adding more sediment to the layer and 2) because bedrock erosion occurs low on the glacier where much sediment transport takes place (Figure 6 d), compared to the *CONST* case. The peak sediment discharge in *CONST* (Figure 5 e, f) occurs slightly earlier in the season, due to the increased amounts of sediment on the glacier's lower portions.

3.2 Griesglestcher

3.2.1 Experiment design

We also simulate Griesgletscher in the Swiss Alps using topographic data from Delaney et al. (2019). Hourly water discharge from the glacier was modeled in Delaney et al. (2018a). Here, we use the discharge time series from 2009–2017. Subglacial sediment discharge from the glacier was determined for four different time periods since fall 2011 by differencing bathymetry maps and considering proglacial erosion quantities (Delaney et al., 2018a). To estimate surface melt across the glacier with respect to elevation, we use,

$$\dot{m}_w(x,y) = \dot{b}^0 + \gamma(z_s(x,y) - z_s^0). \tag{25}$$

Here, γ is the mass balance gradient and z_s^0 represents the glacier's lowest elevation. $\dot{b}^0$ represents the melt rate at the glacier's lowest extent. $\dot{b}^0$ was evaluated numerically at each water discharge value using the hypsometry of the glacier.

We apply a parameter search over a range of values of sediment grain size (D_m, representing a primary control on fluvial transport of subglacial sediment), sliding rate factor (B, representing a control on bedrock erosion), and the initial till height condition (H_0, representing the effects of existing quantities of sediment below the glacier). 100 simulations were run with randomly selected parameters, each with a uniform distribution. No spin up was applied in this case, because of the wide range of H_0 values explored.

The wall time for a single model run averaged $8.9\,\mathrm{h}$, and each run for a parameter set was executed on a single CPU. Instead of applying the mean flotation fraction across the glacier, as was done in the previous cases, the maximum value was applied with an upper limit of 1.

We only considered model outputs resulting in a perfect rank correlation across the four data collection periods and an error less than $131,000\,\mathrm{m}^{-3}$. For the case presented below, we show the simulation with the lowest absolute error between model output and the sediment transport data.

3.2.2 Model outputs and findings

The parameter search yields an optimum grain size parameter D_m of 2 cm, sliding parameter B of 2.05×10^{-11} $\mathrm{MPa\,m\,s^{-1}}$ and initial till height H_0 of $2.5\mathrm{mm}$. The model's ability to reproduce the validation data largely depends on the grain size parameter, D_m. Compared to D_m, the sliding parameters and initial condition parameters (B and H_0) have a reduced influence in representing the data, given that similar values of B and H_0 can produce largely different results in the context of D_m (Figure 7 a, b, c).

The optimized parameter combination, along with others, reproduces the interannual variability in sediment discharge from the Griesgletscher (Figure 7 g). The absolute error between the optimum model run and the measurements is roughly $62,600$ m^3. The error from this parameter search is slightly less than half of the $131,300$ m^3 total sediment discharged from the Griesgletscher over this time period (Delaney et al., 2018a). The model runs captures the third period from late 2014 to late 2015 well. However, the runs systematically overestimate the second and fourth periods and generally underestimate the high discharge period from late 2011 until late 2013 (Figure 7 g).

The best performing model run shows strong temporal variability in sediment discharge. Peaks in sediment discharge occur during the short-lived increases in water discharge (Figure 8 a). Despite the strong dependence on grain size and fluvial transport of sediment in the parameter search, sediment transport capacity Q_{sc} still remains roughly an order of magnitude higher than sediment discharge Q_s (Figure 8 a, b). The steep section of the glacier experiences sediment depletion over the model run, as do several patches of the glacier bed near the over-deepening and high on the glacier (Figure 9 c d). On some parts of the upper glacier, bedrock erosion grows the till layer beyond the initial condition in the absence of substantial sediment transport.

The value of B, from the parameter search, results in an average sliding velocity of $39\ \mathrm{m\ a^{-1}}$, and the range of values for B in the parameter search result in mean sliding velocities roughly between $14\,\mathrm{ma^{-1}}$ and $70\,\mathrm{ma^{-1}}$ (Equation 14). Because sediment production decreases with till height (Equation 12), sediment production is limited to the narrow patches of the glacier bed where minimal till persists and bedrock erosion may occur. As a result, the model requires more sliding to produce the equivalent amount of sediment with more till at the bed, even though the sliding and erosion parameters applied here are within a well constrained range.

4 Model limitations

The lack of knowledge regarding the spatial distribution of subglacial sediment makes selecting an initial value of H difficult. The slow rate of basal erosion means that an equilibrium between fluvial sediment transport and bedrock erosion will likely take centuries to attain, if such an equilibrium may even exist in light of variable climatic, and thus glacier, conditions. Should an equilibrium be present (e.g., Herman et al., 2018; Delaney and Adhikari, 2020), it is probably outside of a feasible computational time of this model given its current processing speeds.

In addition to selecting an initial value of H, we also limit the thickness at which the till must stop accumulating (Equation 6b, H_{lim}) due to changes in the hydraulic potential caused by channel infill of sediment. We assume that this value is on the order of tens of centimeters (Table 2), based upon available observations (Perolo et al., 2018). While the impact of a till layer on bedrock abrasion remains uncertain, we expect that sediment of a certain thickness will armor the bed, preventing erosion (Alley et al., 2003). In turn, we limit erosion with till thickness to a threshold ($5\,\mathrm{cm}$), of the same order as H_{lim} to improve computational time. Additionally, the model does not consider the interactions between fluvial sediment transport and debris concentrations in subglacial ice, which may be important for sub-glacial sediment transport (e.g., Ugelvig et al., 2018).

SUGSET_2D also contains 20 parameters (Table 2 and 3). In the available literature, these parameters have been partially constrained using inverse methods (Brinkerhoff et al., 2016) as well as detailed modeling and measurements (e.g., Chen et al., 2018; Covington et al., 2020; Pohle et al., 2022).

The routing method we use assumes that water flow direction is in response to the Shreve potential (Section 2.3.1). Therefore, it does not explicitly simulate the evolution of efficient and inefficient subglacial drainage systems over the course of the season, or the inheritance of existing subglacial canals or channels (Figure 3; e.g., Werder et al., 2013; Zechmann et al., 2020). Furthermore, a response time of the subglacial channel is chosen prior to simulations to improve computational time, compared to a more sophisticated, but computationally more expensive, representation of processes in an R-channel model (e.g., Röthlisberger, 1972).

5 Implications

Results of both the one-dimensional model (SUGSET; Delaney et al., 2019) and SUGSET_2D highlight the importance of simulating the spatial heterogeneities in bedrock erosion, sediment availability, and sediment transport capacity. Yet, in the one-dimensional version of SUGSET, sediment can be accessed from the till layer across the entire glacier width, perpendicular to the glacier flow line. In SUGSET_2D , sediment access and transport are not averaged over the glacier width. Rather, by considering the spatial distribution in water discharge and sediment availability laterally below a glacier, the model evaluates where heterogeneities may persist and their impact on subglacial sediment dynamics (Figures 6 and 9).

In SUGSET_2D, large diurnal increases in sediment discharge occur near peak daily melt because the area of flowing water expands under the glacier (Figure 5 b, d, f). As a result, increased sediment transport can occur in regions of the glacier bed with substantial sediment when hydraulic conditions permit, then the patch of bed is abandoned when water is routed to another part of the glacier bed (Video supplement). This allows sediment to be stored in these regions until the hydraulic conditions return and increased sediment transport. Such a process is difficult to represent in a one-dimensional model, where the entire width of the glacier is represented together (Figures 4 b and 5 b, d, f; Video supplement). For instance here, diurnal fluctuations in sediment discharge in the middle of the season can be 50% above the mean value (Figure 5 b, d, f), which aligns more closely with some field observation of sediment discharge (e.g., Swift et al., 2005; Delaney et al., 2018b) compared to the one-dimensional version of SUGSET (c.f. Delaney et al., 2019). Furthermore, the results show that the location of bedrock erosion, processes in the till layer, and the timing of melt all play an important role in the quantity of sediment discharge and the peak sediment discharge that is reached.

In the final case, we compared model runs across a parameter space to sediment discharge data from Griesgletscher in the Swiss Alps (Section 3.2). The limited ability of the model to capture the large sediment discharge from the first time period and the minimum sediment discharge in the second and fourth time periods show that processes not adequately represented in the model are responsible for the increase in sediment transport at this time (Figure 7). Such processes may include activation of new patches of the glacier bed or the relocation of channels (e.g., Zechmann et al., 2020), potentially due to changes to glacier surface topography that cause alternative flow paths below the glacier. Furthermore, glacier sliding, remains constant over the model run. In turn, the results do not explicitly account for seasonal or interannual variability in bedrock erosion (e.g., Herman et al., 2015).

Model performance at Griesgletscher depends greatly on sediment grain size, compared to other parameters such as the initial till condition or bedrock erosion (Figure 7). Grain size is a strong control in the SUGSET_2D because it modulates how easily sediment is mobilized in patches of the bed only occasionally accessed by sub-glacial flow during the melt season. This process cannot be fully considered in a one-dimensional model, though this processes seems important on this relatively small and shallow alpine glacier. These results show that connectivity between subglacial channels and distal sediment patches is a strong control on sediment discharge from the subglacial system. This is especially so because main flow paths can be evacuated of sediment (Figure 9 c, d). Thus these flow paths contribute to the catchment's sediment discharge only through the production of sediment through erosion (Equation 12). The connectivity between the main channels and distal sources of sediment could be through the transport of small sediments as applied here, but may also occur through other processes not considered in the model, such as till deformation (e.g., Damsgaard et al., 2020).

Lastly, the model demonstrates the complex nature of subglacial sediment transport and the transitions between supply- and transport- limited regimes. Sediment discharge depends not only on hydrology but also on the sediment availability. Equivalent values of water input and sediment transport capacity below the glacier result in simulated sediment discharge that vary over orders of magnitude (Figure 10 a). In turn, using solely the water discharge or sediment transport capacity (e.g., Equation 8) fails to consider the changes to sediment availability caused by sediment transport, especially when changes to sediment storage can take place over seasons to decades. Finding ways to evaluate these difficult to measure parameters could be key to improving our understanding of subglacial sediment transport.

6 Conclusions

We present a two-dimensional subglacial sediment transport model, SUGSET_2D, that evolves a till layer in response to subglacial hydrology. Model cases utilize geometries and hydrological forcings from a synthetic and a real alpine glacier. The model captures sediment transport in supply- and transport- limited regimes. Results from both cases point to the need to quantify the spatial distribution of subglacial sediment and water when simulating sediment discharge expelled from glaciers. Model outputs reproduce many observed subglacial sediment processes.

Despite the model's ability to reproduce observations, it relies on a large number of poorly constrained parameters. For instance, to our knowledge, only one study has quantified till thickness at a single point below a glacier (Truffer et al., 2000). These observations are limited due to the difficulty of making direct observations at glacier beds. The initial till height, H_0, in the model, therefore, must be chosen thoughtfully because the system remains impacted by this condition throughout the model run.

This two-dimensional sediment transport model can represent several observed characteristics of subglacial sediment discharge compared to the one-dimensional version. SUGSET_2D routes water and sediment using the Shreve potential and a spatially uniform flotation-fraction that evolves in time in the real glacier case (e.g., Section 3.2). Future work may consider using a coupled model of channelized and distributed drainage networks (Hewitt, 2013; Werder et al., 2013). Increasing the sophistication of the subglacial hydrology model may better evaluate the locations of high sediment transport capacity. Such models could even be run offline if the operator assumes, as we do, that rates of change in till height are small compared to the evolution in cross-section of the subglacial conduit.

Our simulations highlight that increased glacier melt does not necessarily result in commensurate changes to sediment discharge unless new previously inaccessible subglacial sediment patches are accessed by meltwater. Additionally, results demonstrate the role of spatially varying water routing and lateral sediment connectivity in subglacial sediment discharge. Further efforts should constrain the role of changing glacial dynamics on erosion and sediment transport. Further modeling and observational studies are needed to better constrain the timescales over-which these processes occur in a changing climate.

Code availability. The code library and illustrative examples are available at https://bitbucket.org/IanDelaney/sugset.jl/src/id-2d. The running and plotting scripts used in the cases herein are stored at https://bitbucket.org/IanDelaney/2d_runners/src/master/.

Video supplement. Videos of a prior model version's application to Griesgletcher are available at https://bit.ly/3nPvVUI, demonstrating model behavior. Similar videos of the current model version will be transferred to a permanent location pending acceptance.

Author contributions. ID designed the study, developed the model, ran the cases and lead writing the manuscript. LA assisted with the writing the manuscript and provided key advice designing and troubleshooting the model. FH provided guidance with implementing and designing the model and preparing the manuscript.

Competing interests. The authors declare no competing interests.

Acknowledgements. We thank J. Braun, B. Bovy, F. De Doncker, G. Jouvet, S. N. Lane, G. Prasicek and M. Werder for fruitful discussions and insightful comments. We are also grateful to Grégoire Mariéthoz and the Scientific Computing and Research Support Unit at Université de Lausanne for providing computing resources. I. Delaney was funded in part by SNF Project No. PZ00P2_202024. I. Overeem, S. Hergarten and two anonymous reviewers provided thoughtful and constructive comments that greatly improved this manuscript.

References

Alley, R. B., Cuffey, K. M., Evenson, E. B., Strasser, J. C., Lawson, D. E., and Larson, G. J.: How glaciers entrain and transport basal sediment: physical constraints, Quaternary Science Reviews, 16, 1017–1038, https://doi.org/10.1016/S0277-3791(97)00034-6, 1997.

Alley, R. B., Lawson, D. E., Larson, G. J., Evenson, E. B., and Baker, G. S.: Stabilizing feedbacks in glacier-bed erosion, Nature, 424, 758–760, https://doi.org/10.1038/nature01839, 2003.

Andersen, J. L., Egholm, D. L., Knudsen, M. F., Jansen, J. D., and Nielsen, S. B.: The periglacial engine of mountain erosion– Part 1: Rates of frost cracking and frost creep, Earth Surface Dynamics, 3, 447–462, https://doi.org/10.5194/esurf-3-447-2015, https://esurf.copernicus.org/articles/3/447/2015/, 2015.

Beaud, F., Flowers, G., and Venditti, J. G.: Modeling sediment transport in ice-walled subglacial channels and its implications for esker formation and pro-glacial sediment yields, Journal of Geophysical Research: Earth Surface, 123, 1–56, https://doi.org/10.1029/2018JF004779, 2018a.

Beaud, F., Venditti, J., Flowers, G., and Koppes, M.: Excavation of subglacial bedrock channels by seasonal meltwater flow, Earth Surface Processes and Landforms, 43, 1960–1972, https://doi.org/10.1002/esp.4367, 2018b.

Bhatia, M. P., Kujawinski, E. B., Das, S. B., Breier, C. F., Henderson, P. B., and Charette, M. A.: Greenland meltwater as a significant and potentially bioavailable source of iron to the ocean, Nature Geoscience, 6, 274, 2013.

Bovy, B., Braun, J., and Demoulin, A.: A new numerical framework for simulating the control of weather and climate on the evolution of soil-mantled hillslopes, Geomorphology, 263, 99 – 112, https://doi.org/https://doi.org/10.1016/j.geomorph.2016.03.016, 2016.

Brinkerhoff, D., Truffer, M., and Aschwanden, A.: Sediment transport drives tidewater glacier periodicity, Nature Communications, 8, 90, https://doi.org/10.1038/s41467-017-00095-5, 2017.

Brinkerhoff, D. J., Meyer, C. R., Bueler, E., Truffer, M., and Bartholomaus, T. C.: Inversion of a glacier hydrology model, Annals of Glaciology, 57, 84–95, 2016.

Chen, Y., Liu, X., Gulley, J. D., and Mankoff, K. D.: Subglacial Conduit Roughness: Insights From Computational Fluid Dynamics Models, Geophysical Research Letters, 45, 11,206–11,218, https://doi.org/10.1029/2018GL079590, 2018.

Church, M. and Ryder, J. M.: Paraglacial sedimentation: a consideration of fluvial processes conditioned by glaciation, Geological Society of America Bulletin, 83, 3059–3072, 1972.

Cook, S., Swift, D., Kirkbride, M., Knight, P., and Waller, R.: The empirical basis for modelling glacial erosion rates, Nature communications, 11, 1–7, https://doi.org/10.1038/s41467-020-14583-8, 2020.

Covington, M. D., Gulley, J. D., Trunz, C., Mejia, J., and Gadd, W.: Moulin Volumes Regulate Subglacial Water Pressure on the Greenland Ice Sheet, Geophysical Research Letters, 47, e2020GL088 901, https://doi.org/https://doi.org/10.1029/2020GL088901, https://agupubs.onlinelibrary.wiley.com/doi/abs/10.1029/2020GL088901, 2020.

Creyts, T. T., Clarke, G. K. C., and Church, M.: Evolution of subglacial overdeepenings in response to sediment redistribution and glaciohydraulic supercooling, Journal of Geophysical Research: Earth Surface, 118, 423–446, 2013.

Cuffey, K. M. and Paterson, W. S. B.: The Physics of Glaciers, Butterworth-Heinemann, Burlington, MA, USA, Forth edn., 2010.

Damsgaard, A., Goren, L., and Suckale, J.: Water pressure fluctuations control variability in sediment flux and slip dynamics beneath glaciers and ice streams, Communications Earth & Environment, 1, 1–8, https://doi.org/10.1038/s43247-020-00074-7, 2020.

de Fleurian, B., Werder, M. A., Beyer, S., Brinkerhoff, D., Delaney, I., Dow, C., Downs, J., Hoffman, M., Hooke, R., Seguinot, J., and Sommers, A.: SHMIP The Subglacial Hydrology Model Intercomparison Project, Journal of Glaciology, 64, 897–916, https://doi.org/10.1017/jog.2018.78, 2018.

Delaney, I. and Adhikari, S.: Increased subglacial sediment discharge during century scale glacier retreat: consideration of ice dynamics, glacial erosion and fluvial sediment transport, Geophyiscal Research Letters, p. e2019GL085672, https://doi.org/10.1029/2019GL085672, 2020.

Delaney, I., Bauder, A., Huss, M., and Weidmann, Y.: Proglacial erosion rates and processes in a glacierized catchment in the Swiss Alps, Earth Surface Processes and Landfroms, 43, 765–778, https://doi.org/10.1002/esp.4239, 2018a.

Delaney, I., Bauder, A., Werder, M. A., and Farinotti, D.: Regional and annual variability in subglacial sediment transport by water for two glaciers in the Swiss Alps, Frontiers in Earth Science, https://doi.org/10.3389/feart.2018.00175, 2018b.

Delaney, I., Werder, M., and Farinotti, D.: A Numerical Model for Fluvial Transport of Subglacial Sediment, Journal of Geophysical Research: Earth Surface, 124, 2197–2223, https://doi.org/10.1029/2019JF005004, 2019.

Egholm, D., Nielsen, S., Pedersen, V., and Lesemann, J.-E.: Glacial effects limiting mountain height, Nature, 460, 884–887, https://doi.org/10.1038/nature08263, 2009.

Egholm, D. L., Pedersen, V. K., Knudsen, M. F., and Larsen, N. K.: Coupling the flow of ice, water, and sediment in a glacial landscape evolution model, Geomorphology, 141, 47–66, 2012.

Engelund, F. and Hansen, E.: A monograph on sediment transport in alluvial streams, Tech. rep., Technical University of Denmark, Copenhagen, Denmark, 1967.

Exner, F. M.: Über die Wechselwirkung zwischen Wasser und Geschiebe in flüssen, Abhandlungen der Akadamie der Wissenschaften, Wien, 134, 165–204, 1920a.

Exner, F. M.: Zur Physik der Dünen, Abhandlungen der Akadamie der Wissenschaften, Wien, 129, 929–952, 1920b.

Felix, D., Albayrak, I., Abgottspon, A., and Boes, R. M.: Suspended sediment measurements and calculation of the particle load at HPP Fieschertal, IOP Conference Series: Earth and Environmental Science, 49, 122 007, https://doi.org/10.1088/1755-1315/49/12/122007, http://stacks.iop.org/1755-1315/49/i=12/a=122007, 2016.

Gimbert, F., Tsai, V. C., Amundson, J. M., Bartholomaus, T. C., and Walter, J. I.: Subseasonal changes observed in subglacial channel pressure, size, and sediment transport, Geophysical Research Letters, 43, 3786–3794, 2016.

Hairer, E., Nørsett, S. P., and Wanner, G.: Solving ordinary differential equations I: nonstiff problems, vol. 1, Springer Science & Business, http://link.springer.com/book/10.1007/978-3-540-78862-1, 1992.

Hallet, B.: A theoretical model of glacial abrasion, Journal of Glaciology, 23, 39–50, 1979.

Hallet, B., Hunter, L., and Bogen, J.: Rates of erosion and sediment evacuation by glaciers: A review of field data and their implications, Global and Planetary Change, 12, 213–235, https://doi.org/10.1016/0921-8181(95)00021-6, 1996.

Harbor, J., Hallet, B., and Raymond, C.: A numerical model of landform development by glacial erosion, Nature, 333, 347, 1988.

Hawkings, J., Wadham, J., Tranter, M., Raiswell, R., Benning, L., Statham, P., Tedstone, A., Nienow, P., Lee, K., and Telling, J.: Ice sheets as a significant source of highly reactive nanoparticulate iron to the oceans, Nature communications, 5, 1–8, https://doi.org/10.1038/ncomms4929, 2014.

Herman, F., Beaud, F., Champagnac, J., Lemieux, J. M., and Sternai, P.: Glacial hydrology and erosion patterns: a mechanism for carving glacial valleys, Earth and Planetary Science Letters, 310, 498–508, https://doi.org/10.1016/j.epsl.2011.08.022, 2011.

Herman, F., Beyssac, O., Brughelli, M., Lane, S. N., Leprince, S., Adatte, T., Lin, J. Y. Y., Avouac, J. P., and Cox, S. C.: Erosion by an alpine glacier, Science, 350, 193–195, https://doi.org/10.1126/science.aab2386, 2015.

Herman, F., Braun, J., Deal, E., and Prasicek, G.: The Response Time of Glacial Erosion, Journal of Geophysical Research: Earth Surface, 123, 801–817, https://doi.org/10.1002/2017JF004586, https://agupubs.onlinelibrary.wiley.com/doi/abs/10.1002/2017JF004586, 2018.

Herman, F., De Doncker, F., Delaney, I., Prasicek, G., and Koppes, M.: The impact of glaciers on mountain erosion, Nature Reviews Earth & Environment, 2, 422–435, https://doi.org/10.1038/s43017-021-00165-9, 2021.

Hewitt, I. and Creyts, T.: A model for the formation of eskers, Geophysical Research Letters, 46, 6673–6680, https://doi.org/10.1029/2019GL082304, 2019.

Hewitt, I. J.: Seasonal changes in ice sheet motion due to melt water lubrication, Earth Planetary Science Letters, 371-372, 16 – 25, https://doi.org/10.1016/j.epsl.2013.04.022, 2013.

Hooke, R. L., Laumann, T., and Kohler, J.: Subglacial Water Pressures and the Shape of Subglacial Conduits, Journal of Glaciology, 36, 67–71, https://doi.org/10.3189/S0022143000005566, 1990.

Humphrey, N. and Raymond, C.: Hydrology, erosion and sediment production in a surging glacier: Variegated Glacier, Alaska, 1982–83, Journal of Glaciology, 40, 539–552, 1994.

Iken, A. and Bindschadler, R. A.: Combined measurements of subglacial water pressure and surface velocity of Findelengletscher, Switzerland: conclusions about drainage system and sliding mechanism, Journal of Glaciology, 32, 101–119, 1986.

Iverson, N. R.: Laboratory simulations of glacial abrasion: comparison with theory, Journal of Glaciology, 36, 304–314, https://doi.org/10.3189/002214390793701264, 1990.

Iverson, N. R.: A theory of glacial quarrying for landscape evolution models, Geology, 40, 679–682, https://doi.org/10.1130/G33079.1, 2012.

Kasmalkar, I., Mantelli, E., and Suckale, J.: Spatial heterogeneity in subglacial drainage driven by till erosion, Proceedings of the Royal Society A: Mathematical, Physical and Engineering Sciences, 475, 20190 259, https://doi.org/10.1098/rspa.2019.0259, 2019.

Koppes, M., Hallet, B., Rignot, E., Mouginot, J., Wellner, J. S., and Boldt, K.: Observed latitudinal variations in erosion as a function of glacier dynamics, Nature, 526, 100–103, 2015.

Lane, S. N., Bakker, M., Gabbud, C., Micheletti, N., and Saugy, J.: Sediment export, transient landscape response and catchment-scale connectivity following rapid climate warming and alpine glacier recession, Geomorphology, 277, 210 – 227, https://doi.org/10.1016/j.geomorph.2016.02.015, 2017.

Li, D., Lu, X., Overeem, I., Walling, D. E., Syvitski, J., Kettner, A. J., Bookhagen, B., Zhou, Y., and Zhang, T.: Exceptional increases in fluvial sediment fluxes in a warmer and wetter High Mountain Asia, Science, 374, 599–603, https://doi.org/10.1126/science.abi9649, 2021.

Li, D., Lu, X., Walling, D., Zhang, T., Steiner, J., Wasson, R., Harrison, S., Nepal, S., Nie, Y., Immerzeel, W., et al.: High Mountain Asia hydropower systems threatened by climate-driven landscape instability, Nature Geoscience, 15, 520–530, 2022.

Mao, L., Dell'Agnese, A., Huincache, C., Penna, D., Engel, M., Niedrist, G., and Comiti, F.: Bedload hysteresis in a glacier-fed mountain river, Earth Surface Processes and Landforms, 39, 964–976, https://doi.org/10.1002/esp.3563, 2014.

Meyer-Peter, E. and Müller, R.: Formulas for bedload transport, in: Hydraulic Engineering Reports, International Association for Hydro-Environment Engineering and Research, 1948.

Milner, A., Khamis, K., Battin, T., Brittain, J., Barr and, N., Füreder, L., Cauvy-Fraunié, S., Gíslason, G., Jacobsen, D., Hannah, D., et al.: Glacier shrinkage driving global changes in downstream systems, Proceedings of the National Academy of Sciences, 114, 9770–9778, 2017.

Nanni, U., Gimbert, F., Vincent, C., Gräff, D., Walter, F., Piard, L., and Moreau, L.: Quantification of seasonal and diurnal dynamics of subglacial channels using seismic observations on an Alpine glacier, The Cryosphere, 14, 1475–1496, https://doi.org/10.5194/tc-14-1475-2020, 2020.

Ng, F. S. L.: Canals under sediment-based ice sheets, Annals of Glaciology, 30, 146–152, 2000.

Paola, C. and Voller, V. R.: A generalized Exner equation for sediment mass balance, Journal of Geophysical Research: Earth Surface, 110, https://doi.org/10.1029/2004JF000274, https://agupubs.onlinelibrary.wiley.com/doi/abs/10.1029/2004JF000274, 2005.

Perolo, P., Bakker, M., Gabbud, C., Moradi, G., Rennie, C., and Lane, S. N.: Subglacial sediment production and snout marginal ice uplift during the late ablation season of a temperate valley glacier, Earth Surface Processes and Landforms, 0, 1–68, https://doi.org/10.1002/esp.4562, 2018.

Pohle, A., Werder, M. A., Gräff, D., and Farinotti, D.: Characterising englacial R-channels using artificial moulins, Journal of Glaciology, p. 1–12, https://doi.org/10.1017/jog.2022.4, 2022.

Prasicek, G., Herman, F., Robl, J., and Braun, J.: Glacial Steady State Topography Controlled by the Coupled Influence of Tectonics and Climate, Journal of Geophysical Research: Earth Surface, 123, 1344–1362, https://doi.org/https://doi.org/10.1029/2017JF004559, 2018.

Prasicek, G., Hergarten, S., Deal, E., Herman, F., and Robl, J.: A glacial buzzsaw effect generated by efficient erosion of temperate glaciers in a steady state model, Earth and Planetary Science Letters, 543, 116 350, https://doi.org/10.1016/j.epsl.2020.116350, 2020.

Quinn, P., Beven, K., Chevallier, P., and Planchon, O.: The prediction of hillslope flow paths for distributed hydrological modelling using digital terrain models, Hydrological processes, 5, 59–79, 1991.

Rackauckas, C. and Nie, Q.: DifferentialEquations. jl–A Performant and Feature-Rich Ecosystem for Solving Differential Equations in Julia, Journal of Open Research Software, 5, 15, https://doi.org/10.5334/jors.151, 2017.

Radhakrishnan, K. and Hindmarsh, A. C.: Description and use of LSODE, the Livermore solver for ordinary differential equations, Reference Publication 1327, NASA, 1993.

Riihimaki, C. A., MacGregor, K. R., Anderson, R. ., Anderson, S. P., and Loso, M. G.: Sediment evacuation and glacial erosion rates at a small alpine glacier, Journal of Geophysical Research: Earth Surface (2003–2012), 110, https://doi.org/10.1029/2004JF000189, 2005.

Röthlisberger, H.: Water pressure in intra– and subglacial channels, Journal of Glaciology, 11, 177–203, 1972.

Seguinot, J. and Delaney, I.: Last-glacial-cycle glacier erosion potential in the Alps, Earth Surface Dynamics, 9, 923–935, https://doi.org/10.5194/esurf-9-923-2021, 2021.

Shields, A.: Anwendung der Aehnlichkeitsmechanik und der Turbulenzforschung auf die Geschiebebewegung, PhD Thesis Technical University Berlin, 1936.

Shreve, R. L.: Movement of water in glaciers, Journal of Glaciology, 11, 205–214, 1972.

Swift, D. A., Nienow, P. W., and Hoey, T. B.: Basal sediment evacuation by subglacial meltwater: suspended sediment transport from Haut Glacier d'Arolla, Switzerland, Earth Surface Processes and Landforms, 30, 867–883, https://doi.org/10.1002/esp.1197, 2005.

Thapa, B., Shrestha, R., Dhakal, P., and Thapa, B. S.: Problems of Nepalese hydropower projects due to suspended sediments, Aquatic Ecosystem Health & Management, 8, 251–257, https://doi.org/10.1080/14634980500218241, 2005.

Truffer, M., Harrison, W. D., and Echelmeyer, K. A.: Glacier motion dominated by processes deep in underlying till, Journal of Glaciology, 46, 213–221, 2000.

Ugelvig, S. V., Egholm, D. L., Anderson, R. S., and Iverson, N. R.: Glacial Erosion Driven by Variations in Meltwater Drainage, Journal of Geophysical Research: Earth Surface, 123, https://doi.org/10.1029/2018JF004680, 2018.

Wadham, J., Hawkings, J., Tarasov, L., Gregoire, L., Spencer, R., Gutjahr, M., Ridgwell, A., and Kohfeld, K.: Ice sheets matter for the global carbon cycle, Nature communications, 10, 1–17, https://doi.org/10.1038/s41467-019-11394-4, 2019.

Walder, J. S. and Fowler, A.: Channelized subglacial drainage over a deformable bed, Journal of Glaciology, 40, 3–15, https://doi.org/10.3189/S0022143000003750, 1994.

Weertman, J.: On the sliding of glaciers, Journal of Glaciology, 3, 33–38, 1957.

Werder, M. A., Hewitt, I. J., Schoof, C. G., and Flowers, G. E.: Modeling channelized and distributed subglacial drainage in two dimensions, Journal of Geophysical Research: Earth Surface, 118, 2140–2158, https://doi.org/10.1002/jgrf.20146, 2013.

Willis, I. C., Richards, K. S., and Sharp, M. J.: Links between proglacial stream suspended sediment dynamics, glacier hydrology and glacier motion at Midtdalsbreen, Norway, Hydrological Processes, 10, 629–648, 1996.

Zechmann, J., Truffer, M., Motyka, R., Amundson, J., and Larsen, C.: Sediment redistribution beneath the terminus of an advancing glacier, Taku Glacier (T'aakú Kwáan Sít'i), Alaska, Journal of Glaciology, p. 1–15, https://doi.org/10.1017/jog.2020.101, 2020.

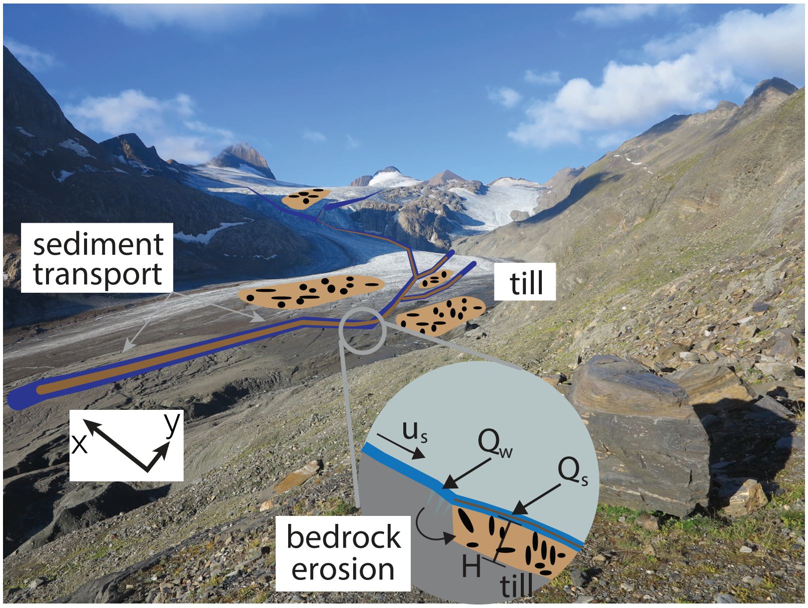

Figure 1. Cartoon of erosional and sediment transport processes considered in model overlaid on image of Griesgletscher in 2016. Bedrock erosion scales with sliding speed (u_s) and adds material to the till layer with thickness H, while water (Q_w) transports sediment (Q_s) fluvially, if sediment persists in that location of the glacier bed and fluvial transport conditions are sufficient.

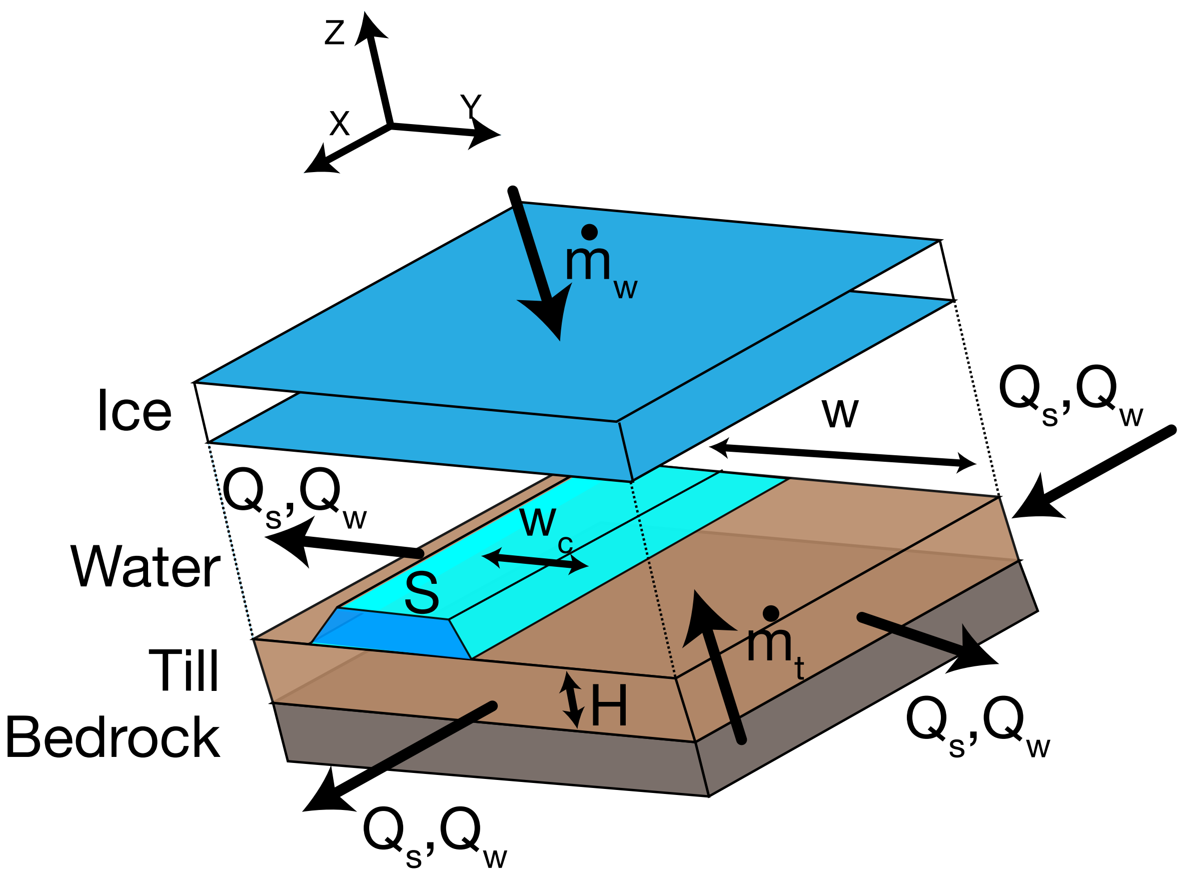

Figure 2. Illustration of terms in Equation 5, detailing the layers of bedrock, till, water and ice. Characteristics of the subglacial channel are also noted, but shown in one dimension for clarity.

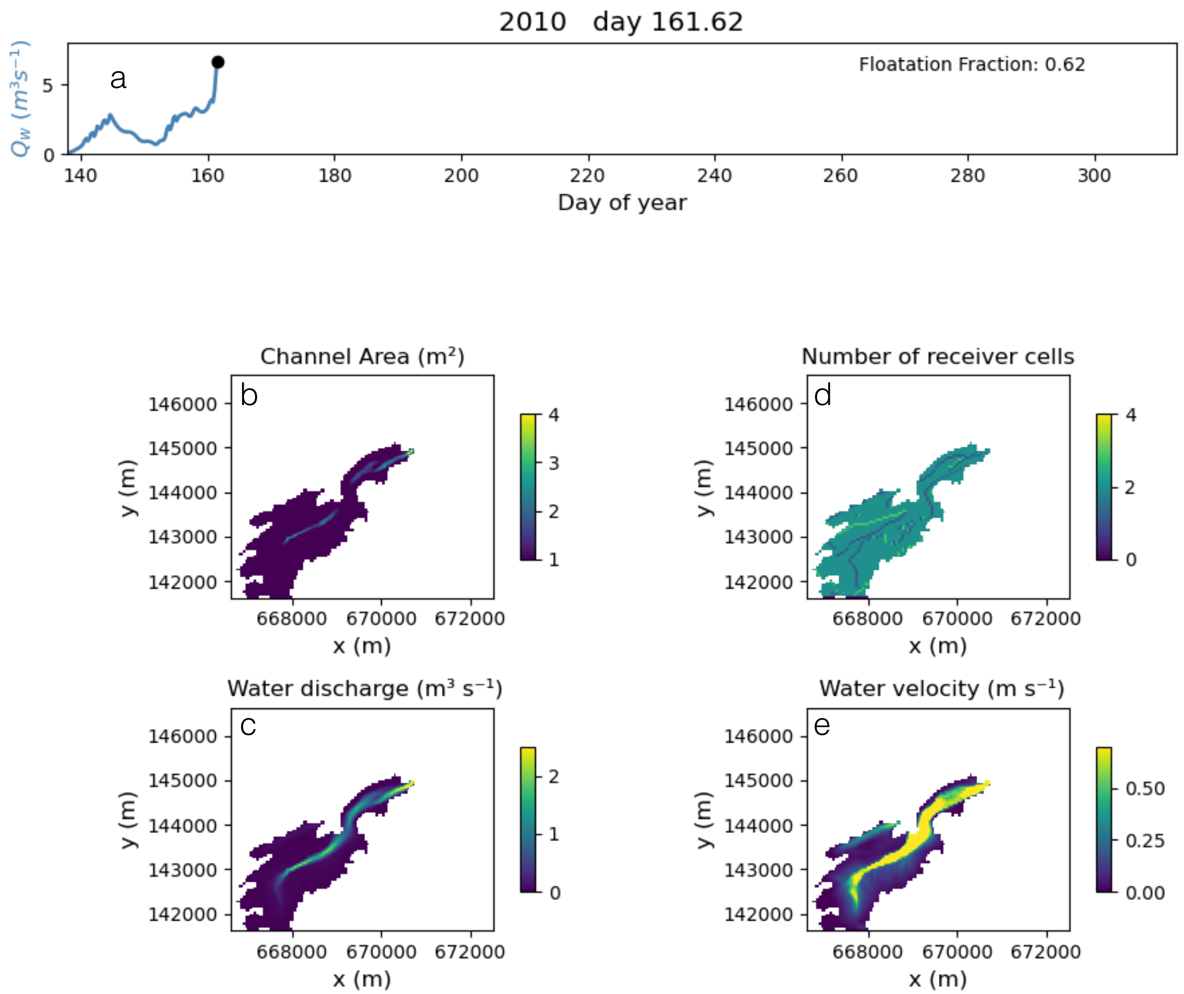

Figure 3. Example of model parameters and variables for the snap shot of the Griesgletscher case Section 3.2. Water discharge from the catchment and glacier flotation fraction (a). Channel cross-sectional area S (b) with distributed water discharge (c), the number of receivers cells, r_t for a given cell (d), and the water velocity (e). Conditions b-e evolve with different hydrological conditions (e.g. a) over the glacier run.

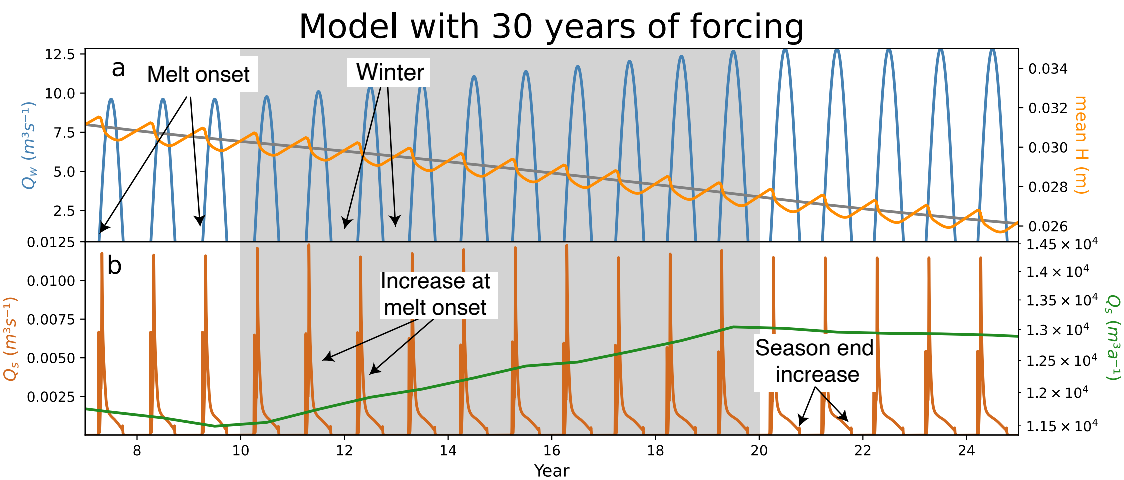

Figure 4. Model output from alpine topography and forcing over a 30 year run with diurnal and seasonal variations in melt input. Grey box represents time period of increasing glacier melt. a) Seasonally varying water discharge (Q_w) increases from year 10 to 20, while till height (H) decreases. b) Annual sediment discharge (green) increases over with increasing melt, with highest sediment discharge occurring in year 19, when glacier melt is greatest. Once the new climate stabilizes, annual sediment discharge stabilizes at a higher level than before.

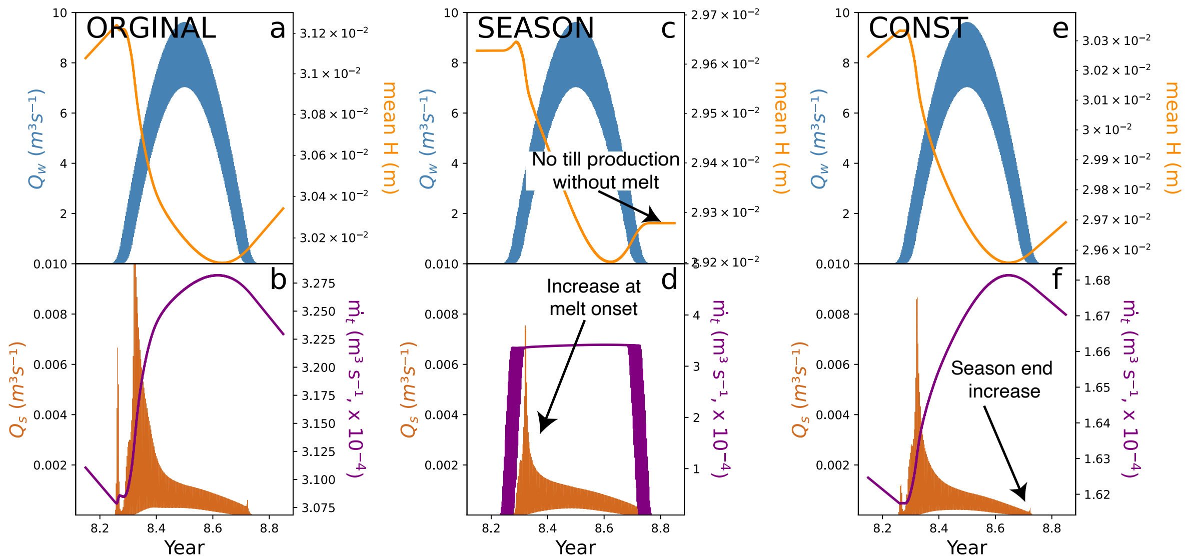

Figure 5. Annual response to different till production patterns across the glacier. (a,b) Conventional model setup, where sediment is produced year-round *ORIGINAL*. (c,d) Equivalent setup to previous, except sediment is only produced in summer months, when water is present at the glacier bed *SEASON*. Note that till height remains constant over the winter months. (e,f) Steady erosion of $1\,\mathrm{mm\ a^{-1}}$ across the entire glacier, with no spatial or temporal variability in sediment production *CONST*.

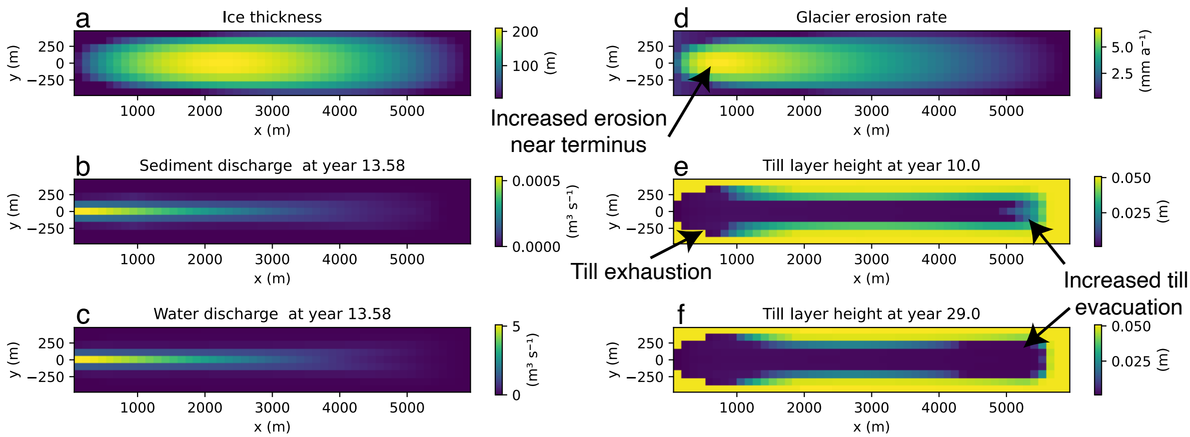

Figure 6. Spatial view of subglacial sediment transport (a), water discharge (c), till layer height prior to increased melt (b) and after increased melt (d). Spatial differences in the distribution of water and sediment discharge in plots a) and c) result from the depletion of subglacial till beneath the glacier. We have included an animation of this figure in the video supplement.

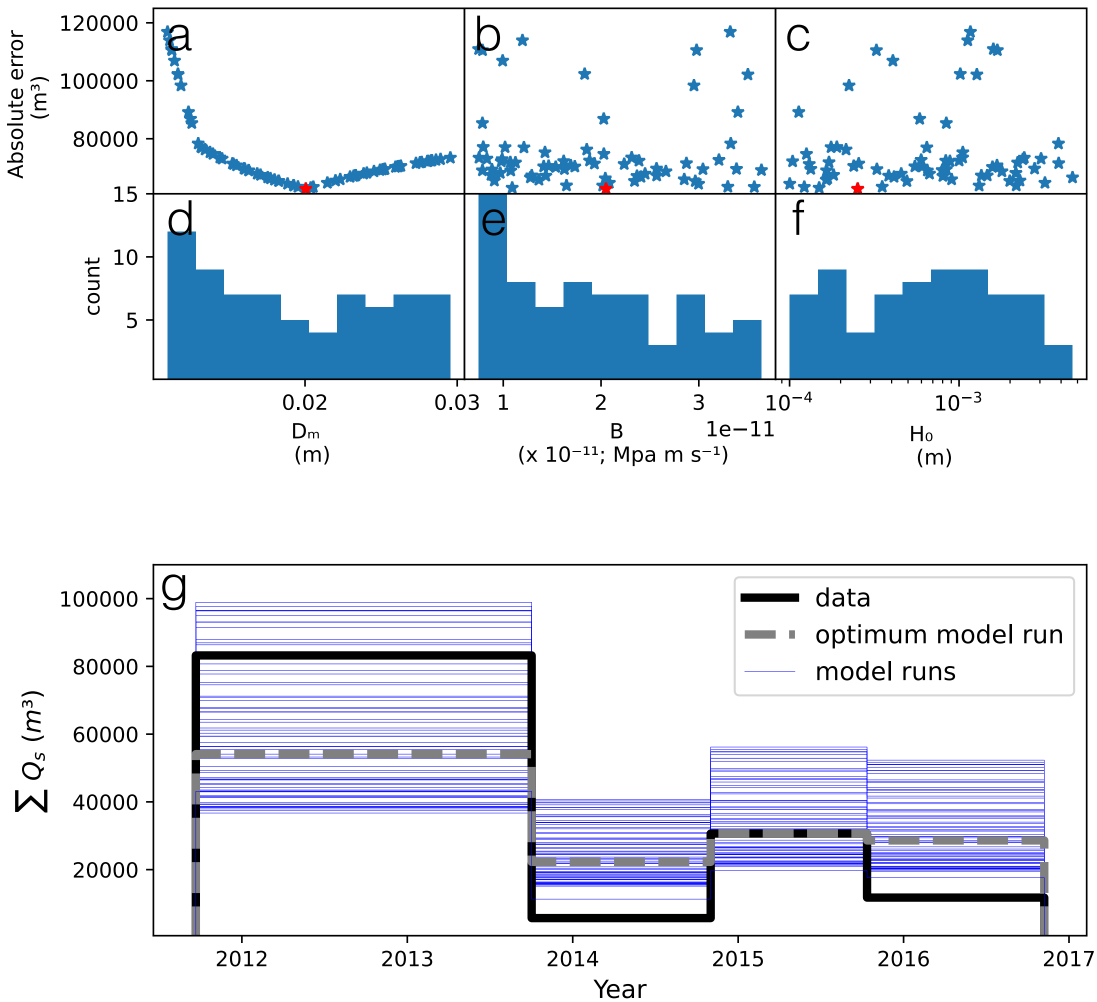

Figure 7. Results of the parameter search (a, b, c), the frequency of parameter values that produced a rank correlation of 1 (d, e, f) and the best fit model run amongst the parameter combinations (g). Red stars represent optimum parameter combination. Blue lines represent all model outputs, while gray line represents the optimum parameter combination.

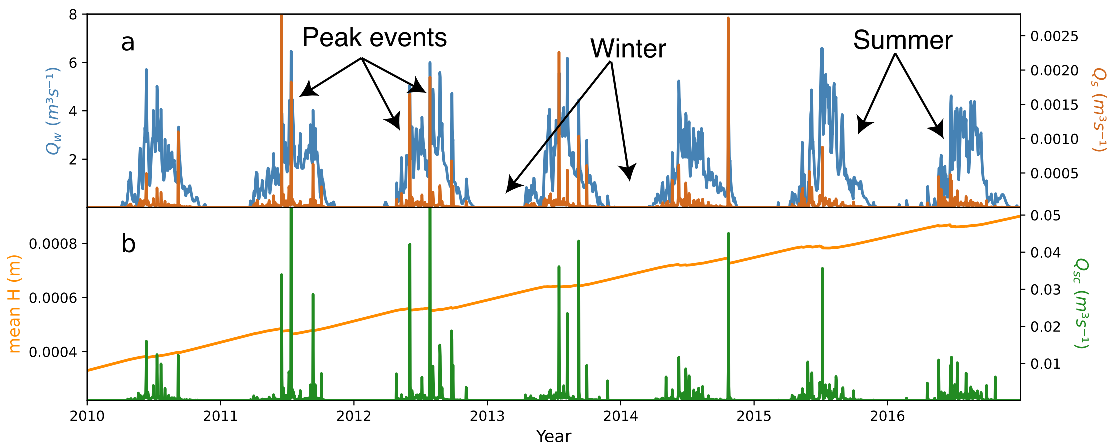

Figure 8. Water discharge, an input modeled for Griesgletscher in (Delaney et al., 2018b), and sediment discharge, output of the model, from Griesgletscher (a). Sediment transport capacity and average till height (b) is below. Note that sediment discharge capacity is roughly one order of magnitude larger than sediment transport discharge. Additionally, the increase in till height H through this model run shows that sediment is produced at a greater rate than it is transported from the glacier bed.

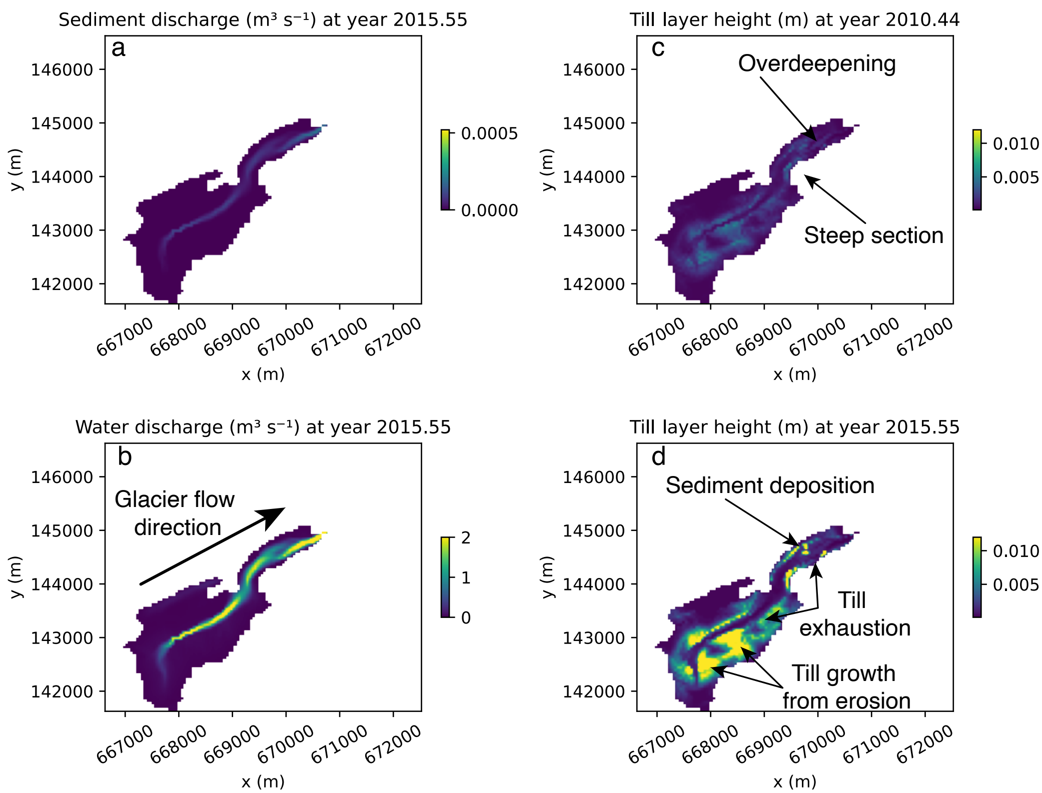

Figure 9. Spatial view of characteristics from the Griesgletscher model run. Figure 1 shows images of this glacier. Subglacial sediment transport (a) and water discharge (c) are highly variable across the bed. Till layer height changes substantially from the beginning of the model run (c) to after the model run (d). We identify the overdeepening near the glacier terminus as well as as a steep section connected the upper and lower glacier. Over this time, till exhaustion in regions of high water flow is visible, while regions of sediment deposition and till growth from glacier erosion can be identified. We have included an animation of this figure in the video supplement.

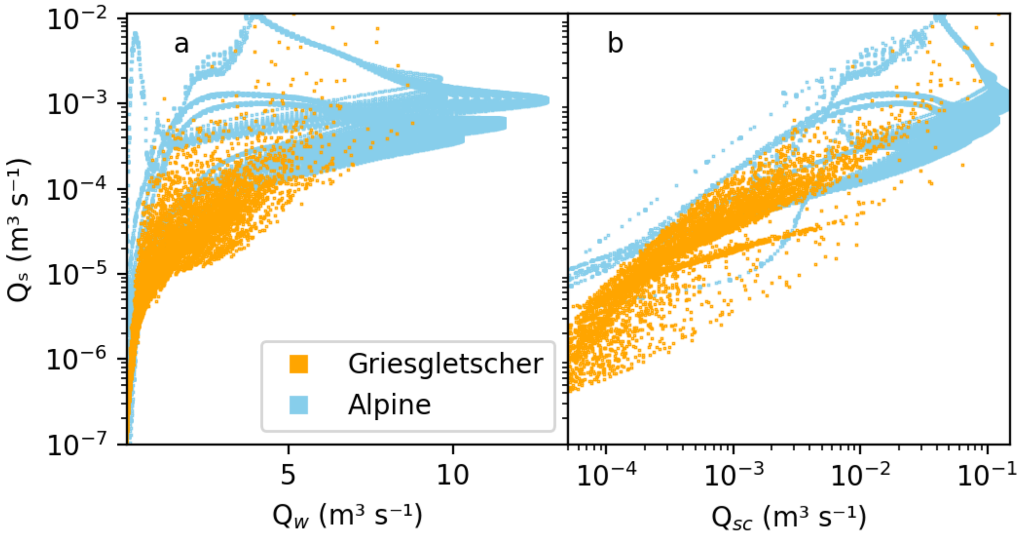

Figure 10. Model outputs of sediment discharge from the glacier compared to water discharge (a) and sediment transport capacity (b).

Table 1. Model variables

Name	**Symbol**	**Units**
Horizontal (x,y) , vertical and time coordinates	x, y, z, t	m, m, m, s
Surface and bed elevation	z_s, z_b	m, m, m
Glacier surface slope	α	-
Channel hydraulic diameter	D_h	m
Width of channel floor	w_c	m
Channel cross-sectional area	S	m^2
Water discharge (instantaneous)	Q_w	$\mathrm{m}^3\,\mathrm{s}^{-1}$
Water source term	$\dot{m}_w$	$\mathrm{m\ s}^{-1}$
Representative water discharge	Q_w^*	$\mathrm{m}^3\,\mathrm{s}^{-1}$
Hydraulic potential	ϕ	Pa
Gradient of ϕ	Ψ	$\mathrm{Pa\ m}^{-1}$
Representative gradient of ϕ	Ψ^*	$\mathrm{Pa\ m}^{-1}$
Flotation fraction	f_f	-
Water velocity	v	$\mathrm{m\,s}^{-1}$
Water shear-stress	τ	Pa
Till source term	$\dot{m}_t$	$\mathrm{m\,s}^{-1}$
Sediment discharge	Q_s	$\mathrm{m}^3\,\mathrm{s}^{-1}$
Sediment discharge capacity	Q_{sc}	$\mathrm{m}^3\,\mathrm{s}^{-1}$
Glacier sliding velocity	u_b	$\mathrm{m\,s}^{-1}$
Basal shear stress	τ_b	MPa
Erosion rate	$\dot{e}$	$\mathrm{m\,s}^{-1}$
Till layer height	H	m
Mass-balance rate at terminus	$\dot{b}^0$	$\mathrm{m\,s}^{-1}$

Table 2. Physical model parameters and constants

Name	Symbol	Value	Units
Darcy-Weisbach friction factor	f_r	Alpine: 15; Gries: 5	-
Hooke angle of channel	β	30	$^\circ$
Source percentile	s_p	Alpine: 0.75; Gries: .2	-
Source average time	s_a	Alpine: 2.5; Gries: 4.5	d
Sediment-uptake e-folding length	l	100	m
Sediment grain mean diameter	D_m	Alpine: 0.01; Gries: 0.02	m
Initial till height	H_0	Alpine:0.05; Gries: 0.0025	m
Till height limit	H_{lim}	0.10	m
Till height erosion limit	H_g	0.05	m
Gravitational constant	g	9.81	$\mathrm{m\,s^{-2}}$
Density of water	ρ_w	1000	$\mathrm{kg\,m^{-3}}$
Density of ice	ρ_i	900	$\mathrm{kg\,m^{-3}}$
Density of bedrock	ρ_b	2650	$\mathrm{kg\,m^{-3}}$
Bulk density of sediment	ρ_s	1500	$\mathrm{kg\,m^{-3}}$
Erosional exponent	l_{er}	2.02	-
Erosional constant	k_g	2.7×10^{-7}	$\mathrm{m}^{1-l_{er}}\ \mathrm{s}^{l_{er}-1}$
Seconds per year	s_{year}	3.1536×10^7	s
Seconds per day	s_{day}	$86,400$	s
Glen's n	n	3	-
Ice flow rate factor	A	2.4×10^{-24}	s Pa^{-3}
Mass-balance gradient	γ	0.00625	a^{-1}
Basal melt rate	$\dot{m}_b$	7.3×10^{-11}	$\mathrm{m\,s^{-1}}$
Sliding rate factor	B	3.2×10^{-12}; Gries: 2.05×10^{-11}	$\mathrm{MPa\,m\,s^{-1}}$
Sliding exponent	m	1	-

Table 3. Numerical model parameters

Name	Symbol	Value	Units
Solver tolerance (relative)	reltol	10×10^{-8}	-
Solver tolerance (absolute)	abstol	10×10^{-8}	m
Maximum timestep	dtmax	21600 (6)	s (hr)
Minimum timestep	dtmin	1	s
Edge length	λ		m
Cell area	δ		m^2
Sediment connectivity factor	$\Delta\sigma$	10^3	m
Minimum hydraulic diameter	Dh_{min}	0.3	m
Number of cells	n_n	-	-
Stack	s_t	$\overrightarrow{n_n}$	-
Receivers	r_s	$4 \times n_n$	-
Number of receivers per cell	n_r	$\overrightarrow{n_n}$	-
Donors	d_n	$4 \times n_n$	-
Number of donors per cell	n_d	$\overrightarrow{n_n}$	-
Weight of each receiver	w_r	$4 \times n_n$	-